Ultrafast Charge Photogeneration Dynamics in Ground-State Charge-Transfer Complexes Based on Conjugated Polymers

Artem A. Bakulin,[†] Dmitry S. Martyanov,[‡] Dmitry Yu. Paraschuk,[‡] Maxim S. Pshenichnikov,*[,†] and Paul H. M. van Loosdrecht[†]

Zernike Institute for Advanced Materials, University of Groningen, Nijenborgh 4, 9747 AG Groningen, The Netherlands, and Faculty of Physics and International Laser Center, Lomonosov Moscow State University, Leninskie Gory, 119991 Moscow, Russia

Received: December 21, 2007; Revised Manuscript Received: August 14, 2008

The charge photogeneration and early recombination in MEH-PPV-based charge-transfer complexes (CTCs) and in MEH-PPV/PCBM blend as a reference are studied by ultrafast visible-pump−IR-probe spectroscopy. After excitation of the CTC band, an immediate (<100 fs) electron transfer is observed from the polymer chain to the acceptor with the same yield as in the MEH-PPV/PCBM blend. The forward charge transfer in the CTCs is followed by an efficient (∼95%) and fast (<30 ps) geminate recombination. For comparison, the recombination efficiency obtained in the MEH-PPV/PCBM blend does not exceed a mere 50%. Polarization-sensitive experiments demonstrate high (∼0.3) values of transient anisotropy for the CTCs polaron band. In contrast, in the MEH-PPV/PCBM blend the dipole moment orientation of the charge-induced transition is less correlated with the polarization of the excitation photon. According to these data, photogeneration and recombination of charges in the CTCs take place locally (i.e., within a single pair of a polymer conjugation segment and an acceptor) while in the MEH-PPV/PCBM blend exciton migration precedes the separation of charges. Results of the ultrafast experiments are supported by photocurrent measurements on the corresponding MEH-PPV/acceptor photodiodes.

1. Introduction

The process of charge photogeneration in conjugated polymer based materials has been actively studied in the last two decades because of its key importance for organic solar cells and photodetectors.[1−3] Charge generation is extremely efficient in polymer−fullerene blends [4,5] which are usually considered as a simple mixture of two compounds without noticeable charge-transfer interaction in the electronic ground state.[1] At the same time, the formation of a weak ground-state charge-transfer complex (CTC) has recently been identified in a number of blends of conjugated polymers with low-molecular weight organic acceptors.[6,7] The donor−acceptor CTCs show high stability[8] and an extended photosensitivity in the red and near-IR ranges due to the presence of a CTC absorption band in the optical gap of the polymer.[6,9,10] Therefore, polymer-based CTCs offer a promising way to develop low-bandgap materials for plastic solar cells and photodiodes. Furthermore, evidence of the formation of a very weak CTC in blends of conjugated polymers with the soluble fullerene derivative PCBM has recently been reported,[11−13] which attracts additional interest to polymer-based CTCs as a model system.

Previous photophysics studies on various low-molecular weight[9,10] and polymer-based[13] CTCs demonstrated that in these materials charge photogeneration and recombination differ considerably from donor−acceptor blends without ground-state charge transfer. As the CTC influences the material properties in a number of ways, one can envisage several reasons for such a difference. First, the CTC photoexcitation formally corresponds to immediate electron transfer from the donor to the acceptor,[14,15] implying that charge separation begins at the very moment of photon absorption. This is in sharp contrast with the bulk-heterojunction concept of conventional donor−acceptor mixture,[3,16] in which an exciton photoexcited either at the donor or acceptor needs to diffuse to the donor−acceptor interface where the charge separation occurs. Second, the donor−acceptor coupling in the CTC might facilitate not only an efficient charge separation but also a geminate recombination,[17,18] hereby reducing availability of charge carriers at long times. Finally, the interaction between the donor and acceptor in CTCs could influence the morphology of the blend,[19] which, for instance, in polymer−fullerene blends, is of paramount importance for efficient charge photogeneration[20] and transport.[21,22] Specifically, CTC can facilitate donor−acceptor intermixing,[19] counteracting phase-separation usually observed in donor−acceptor blends without charge-transfer interaction.[22] Being hardly distinguishable in cw photocurrent experiments,[6,13] most of these effects can be dissected from photoexcitation dynamics at the 0.1−100 ps time scale.

One of the most efficient ways of studying the initial dynamics of photogenerated charges in conjugated polymers is photoinduced absorption (PIA) spectroscopy[23] that nowadays features sub-100-fs time resolution.[24] In a PIA experiment, the time evolution of characteristic absorption bands associated with the photoinduced charges is directly monitored. In PPV-type polymers, these bands include the so-called high-energy (HE) band at ∼1.1 μm,[18,25,26] the low-energy (LE) band around 3.5 μm,[27,28] and the IR active vibrations (IRAV) band around 8−10 μm.[24,29] The LE band is the most suitable one for optical detection of induced charges because, on one hand, the LE band is not contaminated by the presence of stimulated emission, electroabsorption, triplet-state excitation, or ground-state

* Address correspondence to this author. E-mail: m.s.pchenitchnikov@rug.nl.
[†] University of Groningen.
[‡] Lomonosov Moscow State University.

10.1021/jp8048839 CCC: $40.75
Published on Web 10/09/2008

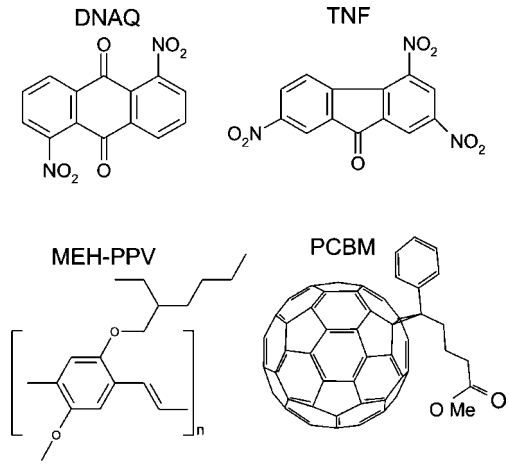

Figure 1. Chemical structures of CTC acceptors (DNAQ, TNF), donor polymer MEH-PPV, and reference acceptor PCBM.

bleaching[30,31] as the widely exploited HE band might be. On the other hand, unlike the IRAV band, it lacks absorption originating from the ground-state vibrational modes of the polymer, thereby allowing for background-free measurements. Another attractive property of the LE band stems from the fact that the orientation of the LE transition dipole is strongly correlated with the orientation of the excitonic absorption dipole of the polymer chain, similar to the HE band.[32] Therefore, polarization-sensitive PIA experiments can provide valuable information on charge and energy transfer among conjugated segments of the polymer. This venue has been exploited only cursorily so far, even for the HE band.[32]

In the current study, we investigate the early time photophysics of polymer-acceptor blends with a pronounced ground-state CTC formation. The CTCs between a MEH-PPV polymer and two acceptors (TNF and DNAQ) with different electron affinities have been used as a model system. PIA spectroscopy on the LE band allowed us to follow the transient absorption changes caused by positive charges on the polymer chains with 100 fs time resolution. After excitation of the CTCs in the visible, an immediate (<100 fs) appearance of the LE band was observed, which is associated with ultrafast formation of charges on the polymer. Although the charge photogeneration in CTCs shows a yield comparable to that in the MEH-PPV/PCBM blend, it is followed by an efficient and fast (<30 ps) geminate recombination. As a result of the recombination, the concentration of long-lived charges in the CTCs appears to be 1 order of magnitude lower than that in a MEH-PPV/PCBM blend. According to the polarization-sensitive experiments, photogeneration and recombination of charges in the CTCs occur locally (i.e., within a single pair of a polymer conjugation segment and an acceptor) in contrast to the MEH-PPV/PCBM blend where ultrafast energy transfer takes place prior to charge generation. The results of the ultrafast optical experiments are in good agreement with external quantum efficiency measurements of photon-to-current conversion, observed in the corresponding MEH-PPV/acceptor photodiodes.

2. Experimental Section

As model CTCs we studied binary mixtures of poly[2-methoxy-5-(2-ethyl-hexyloxy)-l,4-phenylene vinylene] (MEH-PPV) with 2,4,7-trinitrofluorenone (TNF) or 1,5-dinitroantraquinone (DNAQ) (Figure 1a). The MEH-PPV/TNF and MEH-PPV/DNAQ blends were prepared by dissolving each component separately in chlorobenzene with a concentration of 1 g/L. The

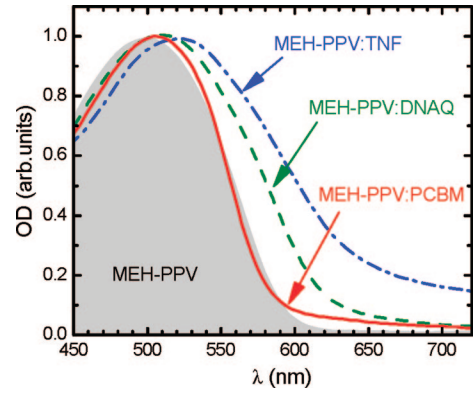

Figure 2. Normalized absorption spectra of MEH-PPV/DNAQ (green dashed curve) and MEH-PPV/TNF (blue dash-dotted curve) CTCs, MEH-PPV/PCBM blend (red solid curve), and pristine MEH-PPV (shaded contour).

solutions were mixed with a weight ratio of MEH-PPV:TNF or MEH-PPV:DNAQ of 1:0.3 to maximize the CTC concentration in the films.[33] Up to this ratio, almost all acceptor is involved in the CTC with no signs of separate acceptor phase formation as follows from difference scanning calorimetry data[34] and Rayleigh scattering data[19] of CTCs with different acceptor concentrations. This conclusion was also confirmed by the AFM topography scans on the studied films (see the Supporting Information).

Films were prepared by drop-casting on 180-μm-thick fused silica microscope cover slides (UQG-Optics). The reference blend of MEH-PPV and the soluble C_{60} derivative (6,6)-phenyl-C_{61}-butyric acid (PCBM) with 40% of fullerene content (by weight) was prepared following the same procedure. Optical densities at the excitation wavelength of the samples were kept below 0.6 to ensure homogeneous excitation along the beam propagation direction. All experiments were performed in ambient conditions as no sample degradation during measurements was observed.

Time and spectrally resolved PIA experiments were performed at two setups optimized for either wide-range IR tunability or high time resolution. The first system was based on a commercially available Ti:sapphire regenerative amplifier (Hurricane, Spectra-Physics) and two optical parametric amplifiers (TOPAS, Light Conversion) operating in the visible (500−700 nm) and IR (1.2−20 μm) regions. The output of the former was used as a pump while the latter provided the tunable IR probe. The polarizations of the pump and probe beams were always parallel. The cross-correlation width for any wavelength combination did not exceed 400 fs.

The second laser system featured a substantially higher time resolution (<100 fs) and a better signal-to-noise ratio at the expense of IR tunability. The output of a home-build 1 kHz Ti:sapphire multipass amplifier pumped a noncollinear optical parametric amplifier (NOPA)[35] and a 3-stages IR OPO.[36] The NOPA followed by a BK7 prism compressor produced 30 fs, 40 nJ excitation pulses tunable over the visible range (500−700 nm). The IR OPO was specially designed to generate short (<70 fs, 350 cm^{-1} fwhm) transform-limited pulses centered at the LE charge-associated band of MEH-PPV at 3 μm.[30] The polarization of the IR probe beam was rotated by 45° with respect to the polarization of the visible pump beam. After the sample, the probe component parallel or perpendicular to the pump was selected by a wire-grid polarizer (1:100 extinction) and detected by a liquid-nitrogen-cooled InSb photodiode.

In both setups, the visible pump beam was focused into a factor of 2 wider spot than the IR beam to minimize the spatial

inhomogeneity of excitation in the probed region. The density of absorbed photons in the sample did not exceed 10^{18} cm^{-3}, which is 1 order of magnitude lower than typically required for exciton−exciton annihilation to affect the dynamics.[37] The IR signal was processed by a lock-in amplifier referenced to a mechanical chopper in the pump beam, and normalized to the averaged power of the transmitted light I to obtain the relative change in transmission:

$$\Delta T = \frac{\Delta I}{I} \quad (1)$$

where ΔI is the difference between the probe beam powers with the pump open/closed. In the polarization-sensitive measurements, the isotropic (population) signal $\Delta T_{Iso}(t)$ and the induced anisotropy $r(t)$ were calculated[38] by using the following expressions:

$$\Delta T_{Iso}(t) = \frac{\Delta T_{\parallel}(t) + 2 \cdot \Delta T_{\perp}(t)}{3} \quad (2)$$

$$r(t) = \frac{\Delta T_{\parallel}(t) - \Delta T_{\perp}(t)}{3 \cdot \Delta T_{Iso}(t)} \quad (3)$$

where $\Delta T_{\parallel}$ and $\Delta T_{\perp}$ are the relative transmission changes for the parallel and perpendicular components of the probe, respectively. Note that upon derivation of eqs 2 and 3, a random three-dimensional distribution of chromophores is assumed. However, anisotropic polymer chain packing was reported in similar blends for directions across and along the film.[39,40] Although this can potentially lead to a slight crosstalk between the isotropic and anisotropic signals, the range of possible anisotropy values from 0.4 (parallel dipole moments) to −0.2 (orthogonal dipole moments) is not affected.[38] A detailed account of data processing and global fitting analysis can be found in the Supporting Information.

In the cw PIA experiments, the sample was excited at the wavelength of 532 nm by the second harmonic of a cw Nd:YAG laser with an intensity of 60 mW/cm^2. For the near-IR measurements a combination of a tungsten−halogen lamp, a monochromator coupled to a Si or cooled InGaAs photodetector, and a lock-in amplifier at 75 Hz modulation frequency was employed. For longer IR wavelengths, an FTIR spectrometer (Infralum FT-801) was used with the successive 32 s acquisition of spectra with and without cw illumination. In the latter measurements, a sample was drop-cast on a IR transparent BaF_2 substrate.

For the photocurrent measurements, sandwich-type samples were prepared on ITO-covered glass substrates. A PEDOT:PSS layer was spin-cast onto the ITO -side. After that, an active layer was spin-cast (1000 rpm) on top of the PEDOT:PSS layer from MEH-PPV/acceptor 5 g/L chlorobenzene solution. The active layer absorbed less than 50% of the incident light (the thickness did not exceed 50 nm) so that the internal filtering effect can be neglected. Then aluminum contacts were thermally deposited onto the active layer. Photodiodes were illuminated through the substrate by a spectrally dispersed tungsten−halogen lamp, and the preamplified photocurrent was measured by a lock-in amplifier at a 75 Hz modulation frequency.

3. Results and Discussion

Figure 2 presents linear absorption spectra of pristine MEH-PPV, MEH-PPV/DNAQ, and MEH-PPV/TNF CTCs, and the MEH-PPV/PCBM blend as a reference. The mixing of the polymer with TNF and DNAQ results in substantial changes of the absorption spectra. First, the absorption edge shifts beyond 600 nm and, second, an absorption wing is formed at about 650 nm and stretches to the near-IR region. Since pristine MEH-PPV, TNF, and DNAQ are transparent in this region, the emerged red absorption was attributed to the CTC bands.[6,33] The enhancement of the red absorption correlates with the acceptor affinities, indicating a stronger charge-transfer interaction in MEH-PPV/TNF than in MEH-PPV/DNAQ. As a result, MEH-PPV/DNAQ and MEH-PPV/TNF CTCs provide a wider absorption range that extends to the red/near-IR spectral region compared to the MEH-PPV/PCBM blend. Similar to the MEH-PPV/PCBM mixture,[1] the fluorescence in the CTCs was quenched by at least 3 orders of magnitude compared to pristine polymer. No subsidiary fluorescence bands corresponding to the CTC radiative relaxation[41,42] were observed in the 600−1800 nm spectral region.

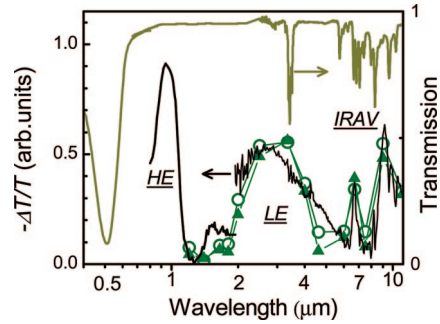

Figure 3. Transient PIA spectrum of MEH-PPV/DNAQ CTC at 1 (open circles) and 50 ps (closed triangles) after the 660 nm excitation. For comparison, the cw PIA spectrum of the MEH-PPV/C_{60} 1:0.1 blend excited at 532 nm is shown by the black curve. The dotted line depicts the transmission spectrum of unexcited MEH-PPV/DNAQ. Following ref 30, IRAV, LE, and HE stand for IR active vibrations and low-energy and high-energy polaron PIA bands, respectively.

To identify optical signatures of the charged states in CTCs, we compared the transient PIA CTC spectra to the well-studied[23,30] charge-associated bands in the MEH-PPV/C_{60} blends. For that, the excitation pulses with a ∼15 nm fwhm bandwidth were centered at a wavelength of 650 nm. This wavelength matches the red flank of the CTC absorption band (Figure 2) thereby causing direct charge separation between the CTC acceptor and donor. In addition, the pristine MEH-PPV polymer is transparent at 650 nm and, therefore, its direct response (if any, vide infra) is excluded.

Figure 3 depicts the time-resolved PIA spectrum of MEH-PPV/DNAQ CTC recorded at 1 ps delay between the pump and probe pulses (circles). For comparison, the cw PIA spectrum of a MEH-PPV/C_{60} blend recorded at the excitation wavelength of 532 nm is also shown as a solid curve. Both spectra exhibit similar features: a broad absorption band at ∼3 μm and several narrower bands at ∼10 and ∼7 μm (not well resolved in the CTC spectrum due to finite time-bandwidth product of the ultrashort pulses). All these PIA bands are known to be characteristic signatures of positive charges on the MEH-PPV chains.[27,30,31] The bands at 1000−1600 cm^{-1} are associated with modifications of IR active vibrational modes while the band at 3000 cm^{-1} is assigned to the LE polaron.[30] Only the cw PIA measurements were extended to observe the HE polaron band at ∼1 μm.

The measured time evolution up to 1 ns was similar for both IRAV and LE bands, which points to their identical origin, namely, the chain deformation due to charge dynamics. As was discussed in the Introduction, despite the readily avoidable CH-stretch lines at ∼3.3 μm, the LE band is free from background absorption (Figure 3, dashed curve), which warrants accurate

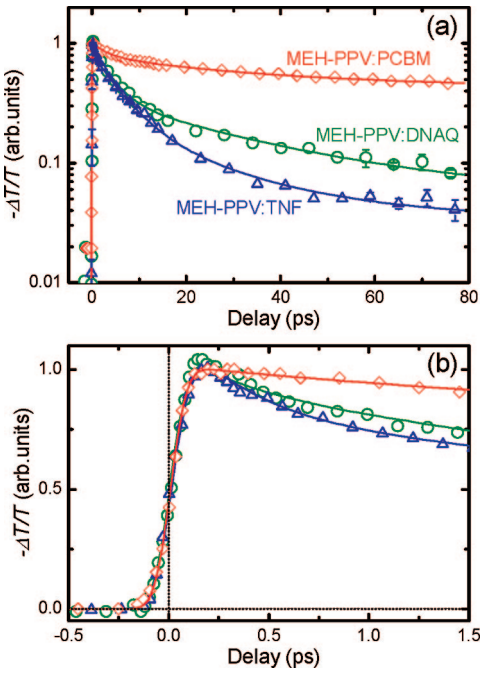

Figure 4. Long (a) and short (b) time isotropic PIA of the LE band in MEH-PPV/DNAQ (green circles) and MEH-PPV/TNF (blue triangles) CTCs excited at 650 nm, and MEH-PPV/PCBM blend excited at 540 nm (red diamonds). Solid curves represent fits to data with parameters given in Table 1, and convoluted with the Gaussian instrument response function. All data are normalized to their maximum value for easier comparison.

differential absorption and anisotropy measurements. In addition, the width of the LE band allows probing with short IR pulses, which enhances the temporal resolution. With this in mind, our attention will be further focused at the LE polaron band as an optical probe for charged states at the MEH-PPV.

In general, the amplitude of the PIA signal is sensitive to the concentration of charges in the polymer and the absorption cross-section (or extinction coefficient). The relaxation of the charged state, environment rearrangement, or other structural processes may lead to a change in the LE transition cross-section. Any sensitivity of the LE transition to relaxation of the charged state should be manifest in the spectral dynamics of the LE transition band. However, the spectra observed in the time interval from 0.5 to 50 ps are identical within the experimental accuracy (Figure 3). Moreover, the CTC PIA spectra follow exactly the cw PIA spectrum of the MEH-PPV/C_{60} blend, indicating a similar origin of the signals both on the picosecond and millisecond time scales. The similarity of PIA spectra at such different times strongly suggests that charge-associated transition frequencies, and most probably their cross sections, do not experience any substantial dynamics. This allows us to assume temporal changes in the magnitude of the transition dipole moment be relatively small. In other words, we regard the transient dynamics of the LE absorption band as mainly originating from the temporal evolution of charge population but not the transition cross-section. Note also that identity of the transient spectra at short and long delays rules out a possible spectral modification of the LE band due to heating of the focal volume by dissipated energy of the pump pulse.

Figure 4 compares the time evolution of the LE PIA band in MEH-PPV/TNF, MEH-PPV/DNAQ CTCs, and MEH-PPV/PCBM blend probed at 3300 cm^{-1}. As before, the CTCs were excited at the wavelength of 650 nm while the MEH-PPV/PCBM blend was excited near the polymer absorption maximum at 540 nm to minimize the effect of a direct PCBM excitation in the red region.[43] The LE band in the MEH-PPV/PCBM blend displays a slow decay with time constants of 3.5 ps (22%), 30 ps (30%), and >1 ns (48%). These parameters were obtained by global multiexponential fitting of the parallel and orthogonal polarization transients as well as anisotropy convoluted with the instrument response function (Table 1 and the Supporting Information). In contrast, the PIA decay in the CTCs occurs mainly within the first 30 ps. Although the weights and the time constants of the fast components are slightly different for both CTCs, the decrease of PIA during the first 30 ps is much more prominent than that in the MEH-PPV/PCBM blend.

If we assume that the charge-associated absorption cross-section does not change in time, the LE PIA band reflects the density of the charged species at the MEH-PPV, and therefore, PIA decay represents the process of charge recombination.[28] The limited PIA decay in the MEH-PPV/PCBM blend is indicative of slow recombination of the photogenerated charges. The obtained 50% efficiency of geminate recombination is in good agreement with the average dissociation probability of bound electron−hole pairs of 42% deduced from the cw photocurrent experiments on PPV:PCBM photovoltaic cells under open-circuit conditions.[44] At the same time, the PIA signal from the CTCs decays remarkably faster, pointing to a rapid decrease of charge density in time. Most likely, the shift of electron density to the acceptor during the excitation in the CTCs is followed by back electron transfer to the donor accompanied by CTC relaxation to the ground state. We can speculate that the three different time scales of 0.3, 4−5, and 20−30 ps with comparable amplitudes (Table 1) reflect a broad distribution of the relaxation rates, which originates from a morphology-related diversity of CTC strengths; however, this hypothesis requires further verification. The observed recombination results in a long-time survival probability of the separated charges in CTCs of around 3% (MEH-PPV/TNF) and 8% (MEH-PPV/DNAQ), which is approximately a factor of 10 lower than in the MEH-PPV/PCBM blend.

Figure 4b presents the PIA evolution at short time delays after excitation. The PIA of MEH-PPV/PCBM blend does not display any fast decay during the first 1 ps, either because of the lack of recombination dynamics or because the charge recombination is compensated for by dissociation of a few long-lived excitons on a subpicosecond time scale. With the experimental time resolution of 100 fs there is no difference in the signal risetime between the CTCs and MEH-PPV/PCBM blends. Similar to previous studies on IRAV[24] and HE polaron bands,[26] the rise of the LE polaron absorption is excellently described by a convolution of the exponentially decaying signal and the apparatus function (Figure 4b, solid lines). Therefore, charge generation after excitation occurs much faster than 100 fs, in all materials. For the MEH-PPV/PCBM blend, this is consistent with the previously measured electron transfer time of 45 fs in MDMO-PPV/PCBM.[45] In general, charge transfer between the donor and acceptor sites might not be the only mechanism of charge generation in the case of MEH-PPV/PCBM blend. In pristine polymers, other processes like charge separation on defects or generation of "spatially indirect" excitons[46] are alternative scenarios for charge generation. However, the efficiency of such processes in pristine polymers does not exceed 10%,[27,24] and becomes negligibly low in blends with high PCBM concentration (as used in the current study).

Despite being incredibly fast, the charge separation in CTCs might still be preceded by some intermediate stages similar, for instance, to the exciton transport in MEH-PPV/PCBM

TABLE 1: Parameters of the Triexponential Fit $\sum A_i \exp(-t/T_i)$ ($i = 1, 2, 3$) of Isotropic PIA Transients and Biexponential Fit $r_0 \sum a_i \exp(-t/\tau_i)$ ($i = 1, 2$) of Transient Anisotropy[a]

	isotropic component				anisotropy			
acceptor	A_1 (T_1)	A_2 (T_2)	A_3 (T_3)	A_0''	r_0	a_1 (τ_1)	a_2 (τ_2)	r_0''
TNF	0.31 (0.3 ps)	0.43 (5.8 ps)	0.26 (22 ps)	0.03	0.29	0.2 (0.7 ps)	0.8 (0.6 ns)	0.4
DNAQ	0.32 (0.3 ps)	0.45 (3.5 ps)	0.23 (35 ps)	0.08	0.29		1.0 (>1 ns)	0.4
PCBM	0.22 (3.5 ps)	0.31 (30 ps)	0.47 (>1 ns)	n.a.	0.18	0.53 (0.5 ps)	0.47 (50 ps)	n.a.

[a] The sum of amplitudes A_i and a_i was normalized to unity. A constant offset A''_0 with the anisotropy value of $r''_0 = 0.4$ was added to the MEH-PPV/DNAQ and MEH-PPV/TNF CTCs data to account for the anisotropy rise at long delays (Figure 5). More detailed information about the model and fitting procedure can be found in the Supporting Information.

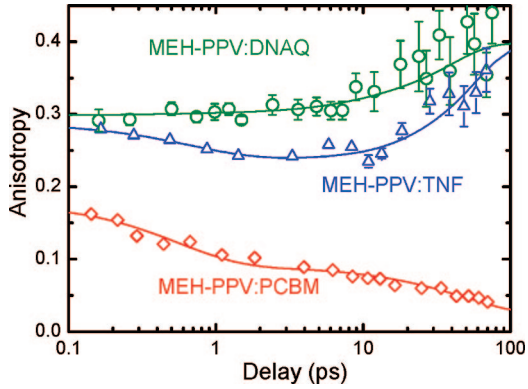

Figure 5. Transient anisotropy decay of the LE polaron band in MEH-PPV/DNAQ (green circles) and MEH-PPV/TNF (blue triangles) CTCs after 650 nm excitation, and in MEH-PPV/PCBM (red diamonds) blend excited at 540 nm. Solid curves are fits to data with parameters given in Table 1. Note the logarithmic scale of the delay axis.

blends. The lifetime of such processes should not exceed 50 fs because they did not result in any noticeable retardation of the isotropic PIA transients (Figure 4b). To address this point in detail, we performed transient anisotropy measurements that are mostly sensitive to the degree of localization of the charge photogeneration.

Figure 5 presents transient anisotropy decays observed in the MEH-PPV/PCBM blend excited at 540 nm and in the CTCs excited at 650 nm. In the reference MEH-PPV/PCBM blend, the anisotropy value amounts to mere $r_0 = 0.18$ (the red diamonds) at 150 fs delay. This is consistent with the loss of polarization memory during exciton migration to the polymer/fullerene interface before charge separation occurs.[16] Being mostly intermolecular, the exciton migration inevitably destroys the memory of the polarization of initial excitation due to the random orientations of dipole moments. The derived value of the initial anisotropy is also similar to one obtained from stimulated emission of DOO-PPV films[27] because the polaron inherits the anisotropy of the parent exciton.

The further decrease of anisotropy at a 0.5 ps time scale can be explained by either continuing deformation of the polymer chain after the excitation or/and polaron migration within the stacked polymer domain, as was recently concluded from pump−probe photocurrent experiments.[32] These processes result in an anisotropy decrease by half—within the first picosecond after excitation. The subsequent slow anisotropy decay (~50 ps) can be assigned to migration of the holes in the polymer because by this time all other processes such as the energy diffusion and charge generation as well as polymer backbone deformation have mostly been completed.[47,48] Thus the most probable reason for the charge-associated transition to change its orientation is polaron hopping from one polymer segment to another one, which has a different orientation of the dipole moment.

Although, to the best of our knowledge, the transient optical anisotropy of the polarons in the MEH-PPV/PCBM blends has never been reported before, its main characteristics corroborate the accepted picture of the exciton and charge dynamics in MEH-PPV/PCBM blends.[16] Note that the anisotropy signal does not depend on charge concentration or absorption cross-section as these two are reduced in the numerator and denominator of eq 3. Also note that anisotropy experiments seem to be a more sensitive probe of charge transport than the isotropic pump−probe transients (Figure 4) as most of the features apparent in the anisotropy remain hidden in the isotropic response. In particular, the 0.5 ps time scale on which the anisotropy decreases by a half is not seen at all in the isotropic transients. This also emphasizes the importance of contrasting the isotropic and anisotropic PIA signals.

The anisotropy in the CTCs (Figure 5, green circles and blue triangles) is persistently higher than that in the MEH-PPV/PCBM blend. For instance, it begins at a value of $r_0 \approx 0.3$ (vs $r_0 = 0.18$ in the MEH-PPV/PCBM blend), which is close to the maximum possible value of 0.4. Note that the anisotropy transients for CTCs indicate no component with a decay time comparable to the temporal resolution. We have previously concluded from the isotropic dynamics that charges on the polymer chain are generated immediately after the excitation, and, therefore, no intermediate "dark" state where the polarization direction could have been scrambled is involved in the charge dynamics. Therefore, a finite angle between the transition dipole moments of the fundamental and the LE polaron transitions is the most obvious and plausible explanation for the lower than 0.4 initial anisotropy. The initial anisotropy value of $r_0 \approx 0.3$ can be recalculated[38] into an (average) angle of ~20° between the dipole moments of fundamental and LE transitions. Alternatively, the initial anisotropy value of 0.3 could result from delocalization of the CTC excitations over several conjugated segments in the presence of high molecular order.[33] The high initial anisotropy value also indicates that the charge separation is confined within the initially excited CTC pair. This is in accord with Mulliken's model of the photoexcited CTC[15] that predicts direct separation of charges between the donor and acceptor upon photoexcitation of the CTC band signifying that energy migration does not play as important a role in CTCs as it does in MEH-PPV/PCBM.

The slight (~20%) decrease of the anisotropy after 0.7 ps observed in the MEH-PPV/TNF CTC only (not in the MEH-PPV/DNAQ CTC) is less prominent that the 50% drop in the MEH-PPV/PCBM blend (for exact values, see Table 1). Therefore, this anisotropy decay in the MEH-PPV/TNF CTC is assigned to continuing deformation of the polymer chain that keeps adapting itself to the excess excitation energy. This is also in line with the absence of a similar decay for the MEH-PPV/DNAQ CTC where the excitation energy excess is lower due to higher energy of the CTC absorption.

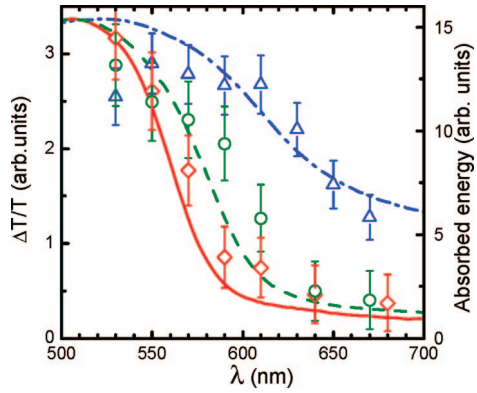

Figure 6. The peak values of the isotropic PIA transients as a function of the excitation wavelength for MEH-PPV/DNAQ (green circles), MEH-PPV/TNF (blue triangles) CTCs, and MEH-PPV/PCBM blend (red diamonds). The energies of the absorbed light are shown as green dashed, blue dash-dotted, and red solid curves, respectively. For direct comparison, the curves were normalized to the absorption maxima at ~510 nm, and the PIA data were rescaled with the same factors. The energy flux of the incident light in all measurements was equal to 15 μJ/cm^2.

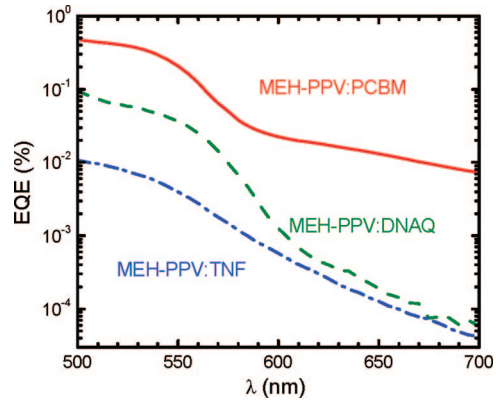

Figure 7. Photocurrent action spectra of MEH-PPV/DNAQ (green dashed curve), MEH-PPV/TNF (blue dash-dotted curve), and MEH-PPV/PCBM blend (red solid curve) photodiodes. The donor:acceptor concentrations are by weight 1:0.3, 1:0.38, and 1:0.4, respectively. EQE stands for external quantum efficiency.

Another striking feature in the anisotropy dynamics is the delayed raise that begins at ~10 ps and reaches the highest possible value of 0.4 at ~100 ps delay. This anisotropy increase cannot be explained within a single CTC ensemble model as it would imply that the memory for the initial polarization is regained after having been lost. This leads us to the conclusion that there are at least two subensembles[49,50] among the excited CTCs. Most of the induced charges have the initial LE transition anisotropy of $r_0 = 0.3$ and 90−95% of them recombine in the first 50 ps, while some of the charges (about 5−10%) live infinitely long (at our experimental time scale) and have a constant anisotropy value of $r'_0 = 0.4$. As the contribution of the former subensemble diminishes in time due to the charge recombination, the latter one becomes more noticeable and finally takes over. Therefore, the transient anisotropy dynamics in CTCs can be explained by the interplay between responses of the short- and long-lived subensembles due to the fact that anisotropy is not an additive value.

The precise origin of the long-lived subensemble cannot be determined solely from the presented spectroscopic experiments. One possible interpretation, based on the previous Raman scattering studies,[33] might be that polymer chains upon the CTC formation straighten and form more ordered domains. This leads, first, to a better correlation in the dipole moment orientation of fundamental and LE electronic transitions and, second, to a steady anisotropy value while the polaron migrates in the polymer domain. The hypothesis of domain formation and higher intermolecular order in CTCs could be tested by grazing angle X-ray diffraction measurements.[51] In any case, the low weight of this subensemble in the overall dynamics undermines its significance for device functionality.

Figure 6 presents the peak values of the isotropic PIA signals (symbols) as a function of the excitation wavelength while the respective energies of the absorbed light are shown as solid curves. The latter were scaled to the identical values at absorption maxima at about 510 nm, and the former were renormalized by using the same scaling factors to ensure direct comparison between the efficiencies of the photon-to-charge conversion in CTCs and MEH-PPV/PCBM. The amplitudes of the peak PIA signals from all samples are similar for excitation around 550 nm, which indicates comparable yield of photon-to-charge conversion within the experimental accuracy. This signifies that the *initial* charge generation is as efficient in CTCs as in the MEH-PPV/PCBM blend, where it is close to unity.[2] In all cases, the peak values of the PIA and therefore amounts of generated charges follow reasonably well the wavelength dependence of light energy absorbed by the sample. Consequently, for the excitation wavelengths above 580 nm, CTCs provide even more charges than MEH-PPV/PCBM. This improved photosensitivity of CTCs originates from the formation of charge-transfer band in the red and near-IR spectral region.

All time-resolved measurements on CTCs were also repeated with the excitation wavelength of 540 nm, i.e. near the absorption maximum of the pristine MEH-PPV (Figure 2). Obtained PIA and anisotropy transients were similar to those depicted in Figures 4 and 5 and will be discussed in detail elsewhere. This invariance in photophysics indicates that the charge-transfer transition is always involved in the CTC excitation. It also confirms the previous observation that for the donor/acceptor ratios used, most of the polymer chains are involved in the CTCs formation.[33,34]

To make a connection between the early stages of photogeneration and the amount of long-lived mobile charges in the studied materials, we performed cw photocurrent experiments on corresponding photodiodes with MEH-PPV/acceptor ratios close to those used in the ultrafast experiments. The photocurrents spectra are presented in Figure 7 in terms of external quantum efficiency (EQE), i.e. the probability of an incident photon to generate a pair of charge carriers at the device electrodes. The photocurrent spectra correlate well with the respective absorption spectra. For instance, in MEH-PPV/TNF and MEH-PPV/DNAQ, the CTC contributes to the photocurrent in the optical gap of MEH-PPV, i.e., for wavelengths longer than 570 nm. Note that in the MEH-PPV/PCBM blends, the photocurrent in this range is determined by the PCBM absorption.[43]

Qualitatively, the EQE in the CTCs is at least 1 order of magnitude lower compared to the reference MEH-PPV/PCBM blend. On the basis of the ultrafast spectroscopy measurements, we attribute such low EQE to the efficient charge recombination and poor charge mobility in the CTC but *not* to ineffective photon-to-charge conversion. The fact that the EQE in the MEH-PPV/DNAQ CTC is higher than that in the MEH-PPV/TNF (Figure 7) is consistent with the less pronounced geminate recombination in the former (consult Figure 4a). However, the geminate recombination alone does not suffice to account for

the observed two-orders-of-magnitude differences in the EQEs of the CTCs and MEH-PPV/PCBM as the concentration of long-lived charges differs only by a factor of ~10 (Figure 4a). Most likely, an additional decrease of photocurrent is caused by low charge mobility as was obtained from the anisotropy measurements. This conclusion is supported by previous studies on the PVK:TNF CTC[52] as well as our photocurrent data for different MEH-PPV:acceptor ratios. In fact, increase of the acceptor content in the MEH-PPV/DNAQ and MEH-PPV/TNF blends beyond 1:0.3 does not considerably change the EQE as it does in the case of the MEH-PPV/PCBM blends due to a dramatic enhancement of charge mobility.[53] Thus, although the initial photon-to-charge conversion in the CTC is as efficient as in PCBM, the fast geminate recombination and low charge mobility do not allow for an efficient charge collection at the device electrodes.

Finally, we discuss potential reasons for the high yield of charge recombination in the CTCs and possible ways to prevent it. The pronounced recombination can arise not only from the donor−acceptor interaction but also from the specifics of the morphology of the material. At the used 1:0.3 donor:acceptor ratio, CTCs show almost completely homogeneous mixing of the compounds with no evidence of separated phases.[19,34] According to the Onsager theory,[54,55] the confinement of photogenerated charges within the parent donor−acceptor pair enhances the recombination probability. Similar effects have previously been observed in other donor−acceptor materials where a low molecular weight donor and acceptor were aggregated,[18] or where a donor chromophore and a fullerene were linked covalently.[17,56] On the other hand, efficient generation of long-lived charges was observed in donor−acceptor blends with charge-transfer interactions but without complete mixing of the donor and acceptor phases.[13] These examples suggest that the recombination efficiency in polymer/acceptor blends might correlate with the absence of donor−acceptor phase separation and the acceptor electron mobility rather than with the CTC formation. If this is the case, the recombination of charges in CTC might be reduced by providing the charge carriers an efficient escape route from the parent CTC, for instance, by using an additional acceptor with high electron mobility (like PCBM).

4. Conclusions

Ultrafast polarization-sensitive VIS-IR spectroscopy has been used to study the photophysics of conjugated polymer-based CTCs and MEH-PPV/PCBM blend. The excitation of the CTC absorption band results in ultrafast (<100 fs) charge generation in CTCs with a yield similar to that in the MEH-PPV/PCBM blend. An efficient (~95%) and fast (<30 ps) geminate charge recombination follows in CTCs while in the MEH-PPV/PCBM blend it does not exceed 50%. The induced anisotropy decay in MEH-PPV/PCBM blend is consistent with intermolecular energy and charge transfer processes that take place at 0.1 and 30 ps time scales, respectively. The efficient charge and energy transfer in the MEH-PPV/PCBM blend are in sharp contrast with CTCs where processes of photoexcitation, charge separation, and recombination appear to be localized within a single donor−acceptor pair. This together with the efficient recombination channels is accountable for the low EQE observed in the corresponding CTC based photodiodes. We believe that potential advantages of CTCs can eventually be combined with efficient photon-to-current conversion if the generated charges are removed from the CTC within 5 ps after the photoexcitation.

Acknowledgment. We are grateful to J. C. Hummelen, M. A. Loi, and V. V. Krasnikov for many useful discussions. J. C. Hummelen is also acknowledged for providing the PCBM. We thank I. V. Golovnin for measurements of the PIA FTIR spectra, E. M. Nechvolodova for help in preparation of photodiodes, L. M. Popescu for assistance with the AFM measurements, and B. Hesp for proofreading of the manuscript. We also acknowledge a suggestion by one of the referees to use the grazing angle X-ray diffraction technique for testing the hypothesis of domain formation and higher intermolecular order in CTCs. This study was in part financially supported by the Russian Foundation for Basic Research (project 07-02-01227-a).

Supporting Information Available: AFM characterization of samples and details of data analysis. This material is available free of charge via the Internet at http://pubs.acs.org.

References and Notes

(1) Sariciftci, N. S.; Smivowits, L.; Heeger, A. J.; Wuld, F. *Science* **1992**, *258*, 1474.
(2) Brabec, C. J.; Sariciftci, N. S.; Hummelen, J. C. *Adv. Funct. Mater.* **2001**, *11*, 15.
(3) Halls, J. J. M.; Pichler, K.; Friend, R. H.; Moratti, S. C.; Holmes, A. B. *Appl. Phys. Lett.* **1996**, *68*, 3120.
(4) Kim, J. Y.; Lee, K.; Coates, N. E.; Moses, D.; Nguyen, T.-Q.; Dante, M.; Heeger, A. J. *Science* **2007**, *317*, 222.
(5) Peet, J.; Kim, J. Y.; Coates, N. E.; Ma, W. L.; Moses, D.; Heeger, A. J.; Bazan, G. C. *Nat. Mater.* **2007**, *6*, 497.
(6) Bakulin, A. A.; Elizarov, S. G.; Khodarev, A. N.; Martyanov, D. S.; Golovnin, I. V.; Paraschuk, D. Yu.; Triebel, M. M.; Tolstov, I. V.; Frankevich, E. L.; Arnautov, S. A.; Nechvolodova, E. M. *Synth. Met.* **2004**, *147*, 221–225.
(7) Panda, P.; Veldman, D.; Sweelssen, J.; Bastiaansen, J. J. A. M.; Langeveld-Voss, B. M. W.; Meskers, S. C. J. *J. Phys. Chem. B* **2007**, *111*, 5076.
(8) Golovnin, I. V.; Bakulin, A. A.; Zapunidy, S. A.; Nechvolodova, E. M.; Paraschuk, D. Yu. *Appl. Phys. Lett.* **2008**, *92*, 243311.
(9) Melz, P. *J. Chem. Phys.* **1972**, *57*, 1695.
(10) Gould, I. R.; Noukalcis, D.; Gomez-Jahn, L.; Young, R. H.; Goodman, J. L.; Farid, S. *Chem. Phys.* **1993**, 176.
(11) Goris, L.; Poruba, A.; Hod′ákova, L.; Vaníček, M.; Haenen, K.; Nesládek, M.; Wagner, P.; Vanderzande, D.; Schepper, L. D.; Manca, J. V. *Appl. Phys. Lett.* **2006**, *88*, 052113.
(12) Goris, L.; Haenen, K.; Nesladek, M.; Wagner, P.; Vanderzande, D.; Schepper, L. d.; D'Haen, J.; Lutsen, L.; Manca, J. V. *J. Mater. Sci.* **2005**, *40*, 1413–1418.
(13) Benson-Smith, J. J.; Goris, L.; Vandewal, K.; Haenen, K.; Manca, J. V.; Vanderzande, D.; Bradley, D. D. C.; Nelson, J. *Adv. Funct. Mater.* **2007**, *17*, 451–457.
(14) Mulliken, R. S. *J. Am. Chem. Soc.* **1950**, *72*, 600.
(15) McGlynn, S. P. *Chem. Rev.* **1958**, *58*, 1113.
(16) Nelson, J. *Curr. Opin. Solid State Mater. Sci.* **2002**, *6*, 87–95.
(17) Vail, S. A.; Schuster, D. I.; Guldi, D. M.; Isosomppi, M.; Tkachenko, N.; Lemmetyinen, H.; Palkar, A.; Echegoyen, L.; Chen, X.; Zhang, J. Z. H. *J. Phys. Chem. B* **2006**, *110*, 14155.
(18) Beckers, E. H. A.; Meskers, S. C. J.; Schenning, A. P. H. J.; Chen, Z.; Wurthner, F.; Marsal, P.; Beljonne, D.; Cornil, J.; Janssen, R. A. J. *J. Am. Chem. Soc.* **2006**, *128*, 649.
(19) Elizarov, S. G.; Ozimova, A. E.; Paraschuk, D. Yu.; Arnautov, S. A.; Nechvolodova, E. M. *Proc. SPIE* **2006**, *6257*, 293.
(20) Beckers, E. H. A.; Chen, Z.; Meskers, S. C. J.; Jonkheijm, P.; Schenning, A. P. H. J.; Li, X.-Q.; Osswald, P.; Wurthner, F.; Janssen, R. A. J. *J. Phys. Chem. B* **2006**, *110*, 16967.
(21) van Duren, J. K. J.; Yang, X.; Loos, J.; Bulle-Lieuwma, C. W. T.; Sieval, A. B.; Hummelen, J. C.; Janssen, R. A. J. *Adv. Funct. Mater.* **2004**, *14*, 425.
(22) Hoppe, H.; Sariciftci, N. S. *J. Mater. Chem.* **2006**, *16*, 45–61.
(23) Sariciftci, N. S.; Smivowits, L.; Wu, R.; Gettinger, C.; Heeger, A. J.; Wuld, F. *Phys. Rev. B* **1992**, *47*, 13835.
(24) Moses, D.; Dogariu, A.; Heeger, A. J. *Chem. Phys. Lett.* **2000**, *316*, 356–360.
(25) Hwang, I.-W.; Soci, C.; Moses, D.; Zhu, Z.; Waller, D.; Gaudiana, R.; Brabec, C. J.; Heeger, A. J. *Adv. Mater.* **2007**, *19*, 2307.
(26) Montanari, I.; Nogueira, A. F.; Nelson, J.; Durrant, J. R.; Winder, C.; Loi, M. A.; Sariciftci, N. S.; Brabec, C. *Appl. Phys. Lett.* **2002**, *81*, 3001.
(27) Sheng, C.-X.; Tong, M.; Singh, S.; Vardeny, Z. V. *Phys. Rev. B* **2007**, *75*, 085206.

(28) Beek, W. J. E.; Wienk, M. M.; Janssen, R. A. J. *Adv. Mater.* **2004**, *16*, 1009.

(29) Mizrahi, U.; Shtrichmana, I.; Gershoni, D.; Ehrenfreund, E.; Vardeny, Z. V. *Synth. Met.* **1999**, *102*, 1182.

(30) Wei, X.; Vardeny, Z. V.; Sariciftci, N. S.; Heeger, A. J. *Phys. Rev. B* **1996**, *53*, 2187.

(31) Osterbacka, R.; Wohlgenannt, M.; Shkunov, M.; Chinn, D.; Vardeny, Z. V. *J. Chem. Phys.* **2003**, *118*, 8916.

(32) Müller, J. G.; Lupton, J. M.; Feldmann, J.; Lemmer, U.; Scharber, M. C.; Sariciftci, N. S.; Brabec, C. J.; Scherf, U. *Phys. Rev. B* **2005**, *72*, 195208.

(33) Bruevich, V. V.; Makhmutov, T. S.; Elizarov, S. G.; Nechvolodova, E. M.; Paraschuk, D. Yu. *J. Chem. Phys.* **2007**, *127*, 104905.

(34) Paraschuk, D. Yu.; Elizarov, S. G.; Khodarev, A. N.; Shchegolikhin, A. N.; Arnautov, S. A.; Nechvolodova, E. M. *JETP Lett.* **2005**, *81*, 583.

(35) Cerullo, G.; Nisoli, M.; Stagira, S.; Silvestri, S. D. *Opt. Lett.* **1998**, *23*, 1283.

(36) Yeremenko, S.; Baltuska, A.; de Haan, F.; Pshenichnikov, M. S.; Wiersma, D. A. *Opt. Lett.* **2002**, *27*, 1171.

(37) Denton, G. J.; Tessler, N.; Harrison, N. T.; Friend, R. H. *Phys. Rev. Lett.* **1997**, *78*, 733.

(38) Gordon, R. G. *J. Chem. Phys.* **1966**, *45*, 1643.

(39) Tammer, M.; Monkman, A. P. *Adv. Mater.* **2002**, *14*, 210.

(40) Zhokhavets, U.; Goldhahn, R.; Gobsch, G.; Al-Ibrahim, M.; Roth, H.-K.; Sensfuss, S.; Klemm, E.; Egbe, D. A. M. *Thin Solid Films* **2003**, *444*, 215–220.

(41) Ruani, G.; Fontanini, C.; Murgia, M.; Taliani, C. *J. Chem. Phys.* **2002**, *116*, 1713.

(42) Loi, M. A.; Toffanin, S.; Muccini, M.; Forster, M.; Scherf, U.; Scharber, M. *Adv. Funct. Mater.* **2007**, *17*, 2111–2116.

(43) Hoppe, H.; Arnold, N.; Sariciftci, N. S.; Meissner, D. *Sol. Energy Mater. Sol. Cells* **2003**, *80*, 105.

(44) Koster, L. J. A. *Device physics of donor-acceptor/blend solar cells*; University of Groningen: Groningen, 2007.

(45) Brabec, C. J.; Zerza, G.; Cerullo, G.; De Silvestri, S.; Luzzati, S.; Hummelen, J. C.; Sariciftci, S. *Chem. Phys. Lett.* **2001**, *340*, 232.

(46) Yan, M.; Rothberg, L. J.; Papadimitrakopoulos, F.; Galvin, M. E.; Miller, T. M. *Phys. Rev. Lett.* **1994**, *72*, 1104.

(47) Westenhoff, S.; Beenken, W. J. D.; Friend, R. H.; Greenham, N. C.; Yartsev, A.; Sundstrom, V. *Phys. Rev. Lett.* **2006**, *97*, 166804.

(48) Brunner, K.; Tortschanoff, A.; Warmuth, C.; Bassler, H.; Kauffmann, H. F. *J. Phys. Chem. B* **2000**, *104*, 3781.

(49) Dokter, A. M.; Woutersen, S.; Bakker, H. J. *PNAS* **2006**, *103*, 15355–15358.

(50) Moilanen, D. E.; Levinger, N. E.; Spry, D. B.; Fayer, M. D. *J. Am. Chem. Soc.* **2007**, *129*, 14311.

(51) Kim, Y.; Cook, S.; Tuladhar, S. M.; Choulis, S. A.; Nelson, J.; Durrant, J. R.; Bradley, D. D. C.; Giles, M.; McCulloch, I.; Ha, C.-S.; Ree, M. *Nat. Mater.* **2006**, *5*, 197.

(52) Gill, D. *J. Appl. Phys.* **1972**, *43*, 5034.

(53) Tuladhar, S. M.; Poplavskyy, D.; Choulis, S. A.; Durrant, J. R.; Bradley, D. D. C.; Nelson, J. *Adv. Funct. Mater.* **2005**, *15*, 1171.

(54) Onsager, L. *Phys. Rev.* **1938**, *54*, 554.

(55) Barth, S.; Bässler, H. *Phys. Rev. Lett.* **1997**, *79*, 4445.

(56) van Hal, P. A.; Janssen, R. A. J.; Lanzani, G.; Cerullo, G.; Zavelani-Rossi, M.; De Silvestri, S. *Chem. Phys. Lett.* **2001**, *345*, 33.

JP8048839

Ultrafast charge photogeneration dynamics in ground-state charge-transfer complexes based on conjugated polymers

- Supplementary Materials -

Artem A. Bakulin[1], Dmitry S. Martyanov[2], Dmitry Yu. Paraschuk[2],

Maxim S. Pshenichnikov[1], Paul H.M. van Loosdrecht[1]

(1) Zernike Institute for Advanced Materials, University of Groningen, Nijenborgh 4, 9747 AG Groningen, The Netherlands

(2) Faculty of Physics and International Laser Center, Lomonosov Moscow State University, Leninskie Gory, 119991 Moscow, Russia

Email: *M.S.Pchenitchnikov@RuG.nl*

1. AFM microscopy characterization of samples

Characterization of the sample surfaces was performed by Tapping mode AFM microscopy. The AFM images were recorded by NanoScope MultiMode Atomic Force Microscope (Digital Instruments) with spatial resolution of 4 nm. Typical surface scans for the samples used in optical studies are presented Fig.A1.

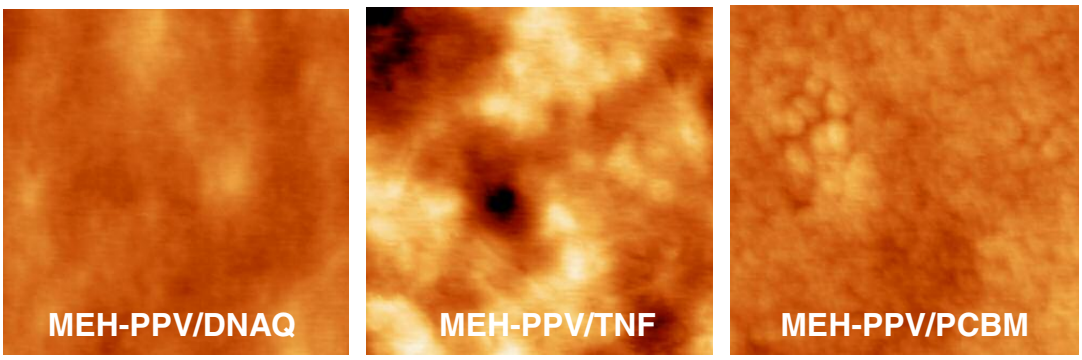

Figure A1. 500x500 nm AFM amplitude images of the studied films. Full color range corresponds to 12 nm in the Z-direction.

2. Data fitting and analysis

The data of the polarization-selective pump-probe experiments were fitted with the following generic model. The PIA signal amplitude was considered to be proportional to the overall concentration of charges N (which also accounts for possible variation in the IR absorption cross-section). The concentration was partitioned between two sub-ensembles N' and N''

$$N(t) = N'(t) + N''(t) \tag{A1}$$

Time evolution of the first sub-ensemble was modeled as a sum of exponential decays to represent the charge concentration and anisotropy, respectively:

$$N'(t) = A_1 \cdot \exp\left(-\frac{t}{T_1}\right) + A_2 \cdot \exp\left(-\frac{t}{T_2}\right) + A_3 \cdot \exp\left(-\frac{t}{T_3}\right) \tag{A2}$$

$$R'(t) = r_0\left[a_1 \exp\left(-\frac{t}{\tau_1}\right) + (1-a_1)\exp\left(-\frac{t}{\tau_2}\right)\right] \tag{A3}$$

where T_i stands for the population relaxation time of the component with the amplitude A_i ($A_3 = 1 - A_1 - A_2$), τ_i is the anisotropy decay time weighted with the amplitude a_i, and r_0 is the initial anisotropy value.

The second ensemble was considered long-lived (at the time scale of our experiment) and possessing a constant anisotropy

$$N''(t) = A_0'' \tag{A4}$$

$$R''(t) = r_0'' \tag{A5}$$

The amplitudes of the parallel $\Delta T_{\parallel}(t)$ and perpendicular $\Delta T_{\perp}(t)$ polarization transients can now be expressed as:

$$\Delta T_{\parallel}(t) = A \cdot \left\{ N'(t) \cdot \left[1 + 2R'(t)\right] + N''(t) \cdot \left[1 + 2R''(t)\right] \right\} \tag{A6}$$

$$\Delta T_{\perp}(t) = A \cdot \left\{ N'(t) \cdot \left[1 - R'(t)\right] + N''(t) \cdot \left[1 - R''(t)\right] \right\} \tag{A7}$$

where A is a normalization coefficient. Making use of Eqs.2 and 3, one can derive the following expressions for the isotropic signal and transient anisotropy:

$$\Delta T_{Iso}(t) = \frac{\Delta T_{\parallel}(t) + 2 \cdot \Delta T_{\perp}(t)}{3} = A \cdot \left[N'(t) + N''(t)\right] \tag{A8}$$

$$r(t) = \frac{\Delta T_{\parallel}(t) - \Delta T_{\perp}(t)}{3 \cdot \Delta T_{Iso}(t)} = \frac{N'(t) \cdot R'(t) + N''(t) \cdot R''(t)}{N'(t) + N''(t)} \tag{A9}$$

As can be seen from Eq.A8, the isotropic transient is free of contamination by reorientational dynamics, i.e. directly proportional to the charge concentration. In contrast, the anisotropy calculated according to Eq.3, is presented by a mixture of purely reorientational and

concentration-related contributions. This reflects the fact that the anisotropy is not an additive quantity and therefore can not be analyzed as such. However, if one of the sub-ensembles dominates (for instance, $N'(t) >> N''(t)$), the concentration contribution drops out:

$$r(t) = R'(t) \tag{A10}$$

Nevertheless, under the circumstances the anisotropy dynamics should be analyzed only together with the population kinetics.

Following this route, we fitted simultaneously the transients measured with parallel and perpendicular polarization, and the anisotropy transients. For that, the expressions given by Eqs.A6 and A7 were convoluted with the instrument response function (a Gaussian with a 100 fs FWHM). We found that inclusion of anisotropy into the fitting routine enhances greatly the accuracy at long times, i.e. where the PIA signals are relatively weak. The results of such a global fit procedure are depicted in Figs.A2 and A3 while the fit parameters are presented in Table 1. As can be concluded from these figures, the model reproduces all essential features of the experimental data. The anisotropy values at long times presented in Fig.5, are averaged over 5 adjacent points.

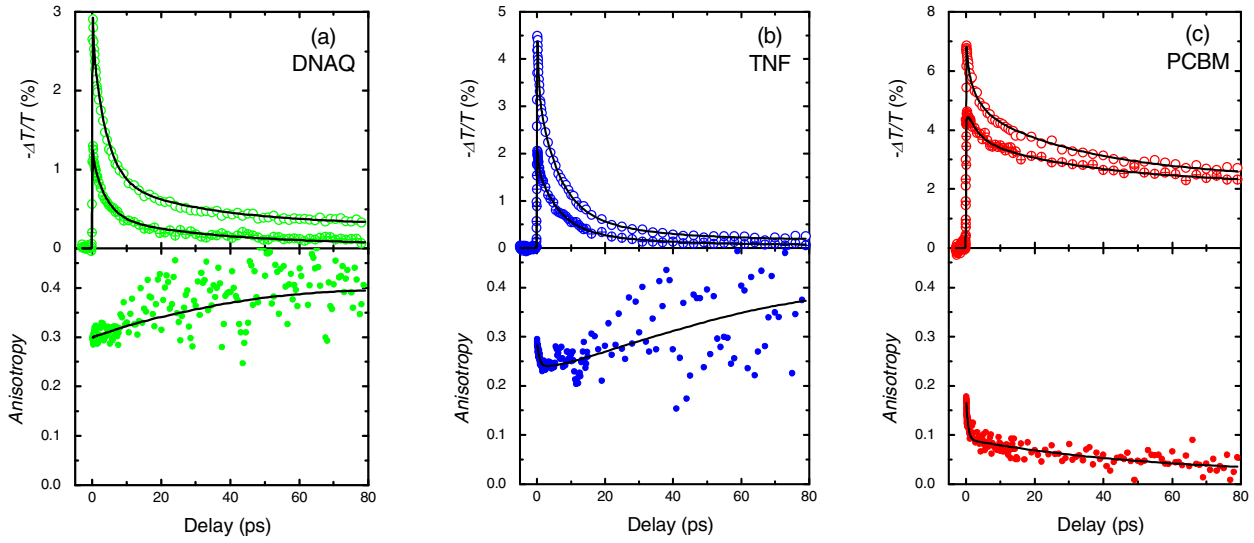

Figure A2. Top panels: absorption transients measured in parallel (open circles) and perpendicular (crossed circles) polarizations between the pump and probe beams in MEH-PPV/DNAQ (a) and MEH-PPV/TNF (b) CTCs excited at 650 nm, and in MEH-PPV/PCBM (c) excited at 540 nm. Bottom panels: corresponding transient anisotropies. Symbols and solid curves show experimental data points and best fits, respectively.

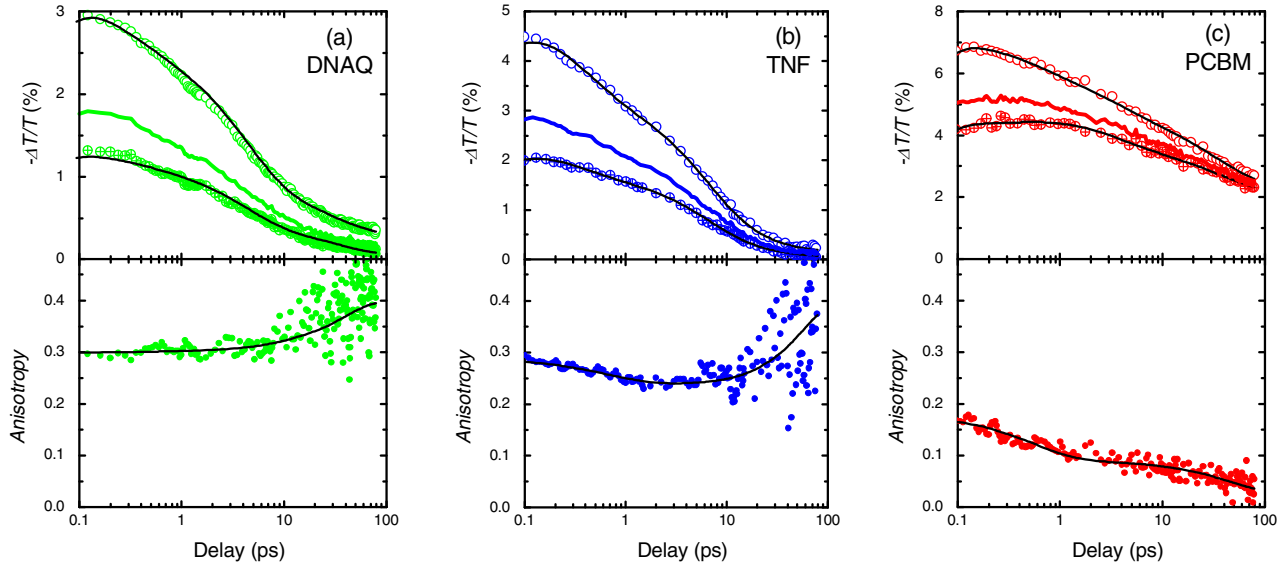

Figure A3. The same as Fig.A2 but presented at the logarithmic time scale. Thick solid curves on the top plots show the isotropic data.